Faraday Discussions

Accepted Manuscript

This manuscript will be presented and discussed at a forthcoming Faraday Discussion meeting. All delegates can contribute to the discussion which will be included in the final volume.

Register now to attend! Full details of all upcoming meetings: http://rsc.li/fd-upcoming-meetings

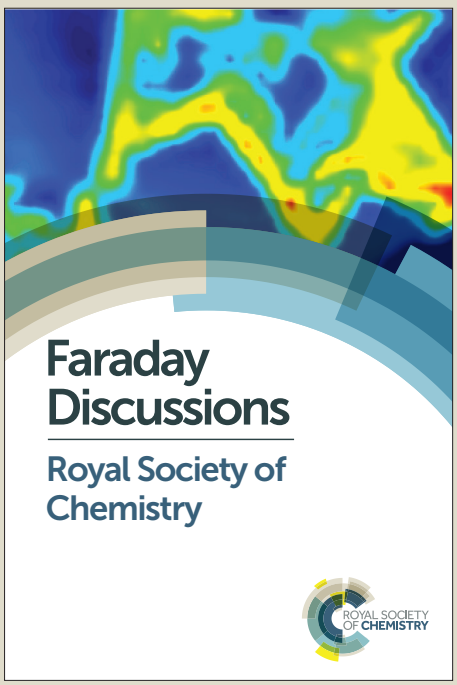

This is an *Accepted Manuscript*, which has been through the Royal Society of Chemistry peer review process and has been accepted for publication.

Accepted Manuscripts are published online shortly after acceptance, before technical editing, formatting and proof reading. Using this free service, authors can make their results available to the community, in citable form, before we publish the edited article. We will replace this *Accepted Manuscript* with the edited and formatted *Advance Article* as soon as it is available.

You can find more information about *Accepted Manuscripts* in the Information for Authors.

Please note that technical editing may introduce minor changes to the text and/or graphics, which may alter content. The journal's standard Terms & Conditions and the Ethical guidelines still apply. In no event shall the Royal Society of Chemistry be held responsible for any errors or omissions in this *Accepted Manuscript* or any consequences arising from the use of any information it contains.

ROYAL SOCIETY OF CHEMISTRY

www.rsc.org/faraday_d

An integrated system for optical and electrical detection of single molecules/particles inside a solid-state nanopore

Xin Shi[a], Rui Gao[a], Yi-Lun Ying[a], Wei Si[b], Yunfei Chen[b], Yi-Tao Long[a]*

[a] Key Laboratory for Advanced Materials and Department of Chemistry, East China University of Science and Technology, Shanghai, 200237, P. R. China.
[b] Jiangsu Key Laboratory for Design and Manufacture of Micro-Nano Biomedical Instruments, Southeast University, Nanjing 210096, China
* To whom correspondence should be addressed: ytlong@ecust.edu.cn

Nanopore techniques have proven to be useful tools for single-molecule detection. The combination of optical detection and ion current measurements enables the new possibility for the parallel readout of multiple nanopores without complex nanofluidics and embedded electrodes. In this study, we developed a new integrated system for the label-free optical and electrical detection of single molecules based on a metal-coated nanopore. An entire system containing a dark-field microscopy system and an ultralow current detection system with high temporal resolution was designed and fabricated. An Au-coated nanopore was used to generate the optical signal. Light scattering from a single Au-coated nanopore was measured under a dark-field microscope. A lab-built ultralow current detection system was designed for the correlated optical and electrical readout. This integrated system might provide more direct and detailed information on single analytes inside the nanopore compared with classic ion current measurements.

1 Introduction

Over the past two decades, nanopore-based techniques have proven to be useful tools for single-molecule detection. Nanopore techniques have become the most promising method for next-generation DNA sequencing[1-3]. In recent years, nanopores have been applied to many fields, such as the structural probing of peptides[4], polymers[5], protein-binding events[6], and the detection of small molecules and host-guest interactions[7-9]. Nanopore-based techniques can provide single-molecule properties during a dynamic process by driving an individual molecule that is traversing through a nanoscale channel. This characteristic enables the investigation of inter- and intramolecular interactions at the single-molecule level dynamically[7, 10].

The core component of a typical nanopore setup is a nanoscale channel with a minimum diameter ranging from a few nanometers to several hundred nanometers. Conduction can only occur through a single nanochannel, which connects two chambers of an electrolyte separated by an insulating membrane. After a voltage bias is applied, a stable ionic current through the single channel (open-pore current) can be generated and recorded by a patch clamp[11, 12]. If a charged analyte is electrophoretically driven through the nanopore, then a measurable current is induced[13]. Generally, the modulation of the ionic current results from the volume exclusion of the analyte, which is often defined as the "ionic-current blockade". By analyzing the duration and the amplitude

of each blockade signal, physical information of an individual analyte can be determined.

The first nanopore-based sensor reported was composed of a single α-hemolysin (α-HL) with a constriction of 1.4 nm at the narrowest point[14]. To detect different analytes and to increase the sensitivity of the nanopore-based sensor, various membrane proteins have been studied, including areolysin[15], MspA[16, 17], ClyA[17], FhuA[18], membrane-adapted phi29 motor protein[19], and SP1[20]. In addition to biological nanopores, there is another category of nanopores known as solid-state nanopores, which are fabricated on thin solid-state membranes by industry standard semiconductor processing techniques, such as an ion/electron beam[21]. A dielectric material, such as low-stress silicon nitride (SiN_x), supported on silicon frames might be the most widely used substrate for drilling the nanopore[12]. Solid-state nanopores could also be fabricated on other high-performance materials, such as SiO_2[22], Al_2O_3[23] and graphene[24-26]. Modern industrial processing allows for the parallel production of nanopore chips and control of the nanochannel geometry.

Although an abundant amount of information can be deduced from the ionic current signal, ionic current-based nanopore methods still face challenges. For example, many signals from single-analyte events should be acquired for statistical analysis due to the randomness of nanopore-based single-molecule detection. To accelerate the measurements, a multichannel nanopore array could be introduced so that a parallel readout of multiple pores can be achieved by measuring the ionic current from each nanopore. Several studies on multiplexing detection have been performed on α-HL nanopores[27, 28] and solid-state nanopores[29]. To simultaneously record an electrical signal from hundreds to thousands of channels, advanced microfluidics and complex circuits are required, thus enlarging and complicating the measurement system. Moreover, information about the species or chemical states of an analyte could not be obtained from the readout of the ionic current. Thus, it would be difficult to identify the species of analytes, which would hinder the application of nanopore-based methods in analyzing complex samples, such as clinical samples.

Optical approaches, in this case, are attractive methods to solve these problems. Detecting optical signals from multi-nanopore channels simultaneously provides a novel multiplexed method without the demand of an individual amplifier circuit for each nanopore[30-33], which allows for a simple and compact instrument and a scaled-down microfluidic system. Optical signals could also reveal chemical states and properties of the specific analytes inside the nanopore. Recently, the translocation events of a single labeled analyte were detected by epi-fluorescence or total internal reflection fluorescence microscopy. The first proof-of-principle study of a single labeled DNA was accomplished in 2007 by integrating a nanopore with single-molecule fluorescence [34]. Since then, fluorophores on different subsets of ds-DNA have been detected by two-channel optical readouts[31]. In addition to fluorescence-based techniques, vibrational spectroscopy methods, such as surface enhanced Raman spectroscopy, have also been introduced for nanopore readouts[35]. Dye-coated gold nanoparticles were driven through a solid-state nanopore with a gold layered membrane, generating electromagnetic 'hot spots' between the particle and the wall of the metallic nanopore, which increased the surface-enhanced resonance Raman scattering (SERRS) signal from the analytes. As a result, the translocation events of a single nanoparticle could be detected by monitoring the characteristic band in the SERRS spectrum. These spectroscopy-based methods provide the possibility of identifying the molecular structures of different analytes by obtaining their corresponding vibrational spectra while recording their nanopore events simultaneously.

Although labeling approaches have increased the specificity of nanopore analysis, the bleaching of the fluorescent dyes and imperfect labeling can influence the detection. Moreover, the

requirement for labeling places a restriction on the sample. Therefore, label-free methods for nanopore-based optical detection have been recently proposed. For example, "optical patch clamping"[36], a method based on calcium imaging, has been introduced to monitor the actions of a single-ion channel. Fluorescent dyes sensitive to Ca^{2+} are used in the electrolyte solution to analyze the concentration of Ca^{2+} in real time. Therefore, as Ca^{2+} ions flow from one side of the pore to the other side, the intensity of the ionic current can be converted into the intensity of fluorescence at a small region around the nanopore. Recently, this method has been successfully applied in solid-state nanopores and has been used for solid-state nanopore readouts[37, 38].

To integrate the advantages of optical and electrical readouts, the synchronized optical and electronic detection of nanopores not only reveals the volume and electrical information but also identifies the structures, conformation and compositions of the analytes. This is especially important for the application of a nanopore to complex samples. Synchronized optical and electrical detection of biomolecules was first achieved by an integrated system based on total internal reflection fluorescence excitation with a high temporal resolution of up to 1000 frames per second[35]. A correlated electrical and optical analysis of single nanoparticles and viruses has been demonstrated based on liquid-core anti-resonant reflecting optical waveguides (ARROWs)[39]. To simultaneously acquire optical and electronic signals at a high bandwidth and high laser power, a low noise nanopore platform based on a Pyrex substrate and a silicon nitride membrane has been developed to reduce the background signal[40]. Meanwhile, the "optical patch clamping" methods have also been applied to simultaneous optical and electronic detection on a solid-state nanopore without labeling of the analyte[37, 38].

Although fluorescence methods have already represented a large portion of nanopore optical detection, the introduction of a fluorophore, either with the labeling procedure or not, would additionally influence the translocation process and the complexity of the experiment. Therefore, an alternative optical approach that does not introduce any additional molecules into the nanopore detection system would be preferable.

Subwavelength apertures have been studied for several years because of their fascinating properties[41], such as strongly enhanced transmission of light and wavelength filtering due to the interaction between light and the surface of the metal film. According to H. A. Bethe, an idealized subwavelength hole on a perfectly conducting metal screen of zero thickness would very weakly transmit light because light with a wavelength longer than the cutoff wavelength (λ) would not propagate through the hole[42]. Optical imaging methods beyond the diffraction limit have been developed based on his theory, such as near-field optical microscopy (NSOM) [43]. At the end of last century, the extraordinary transmission phenomenon through subwavelength holes was reported[44]. Orders of magnitude more light than that predicted by Bethe could be transmitted through an array of tiny holes or through a single subwavelength hole[44] because of surface plasmons, which are generated by the interaction between free electrons of the metal and electromagnetic waves. Furthermore, light could be diffracted, and its direction of propagation could be regulated by sculpting the surrounding material at the wavelength scale[45]. The spectrum of transmitted light could also be regulated by changing the geometry of the nanoscale aperture [44].

The nanoscale aperture has often been used in near-field optical microscopes to excite or collect optical signals from the subwavelength region beyond the diffraction limit. In the last decade, nanoholes in a metal film have also been used to detect single fluorescent biomolecules at high concentrations and have even achieved single-molecule sequencing, known as a zero mode

waveguide[46, 47]. Based on the surface plasmon generated around the nanopore, metal nanopores have also been used as biosensors on the bulk[48, 49] and single-molecule scale[50].

By exploiting subwavelength apertures with plasmonic effects, we developed a new nanopore detection method for the simultaneous acquisition of optical and electrical readouts without the requirement of additional dyes. Our method is based on a single nanopore on a metal-coated silicon nitride (SiN_x) substrate, which can guide the incident light through the nanopore by generating surface plasmons at the edge of the nanopore. An integrated system was designed for simultaneous optical and electrical detection. As shown in Fig. 1, a dark-field microscopy system was used to increase the signal-to-noise ratio of diffracted light through the metal-coated solid-state nanopore. A flow cell acts as a port for connecting the two readouts. The detectors are designed to acquire the optical and electrical signal. A high-speed data acquisition system monitors the variations of optical and ionic current signals simultaneously. We believe that such a strategy could provide more direct and detailed information from single analytes inside the nanopore compared with the classic ionic current measurements.

2 System Composition

Our lab-built system is composed of three main parts: the dark-field microscopy system (Fig. 1a), the ultralow current acquisition system (Fig. 1b) and the metal-coated solid-state nanopore (Fig. 2).

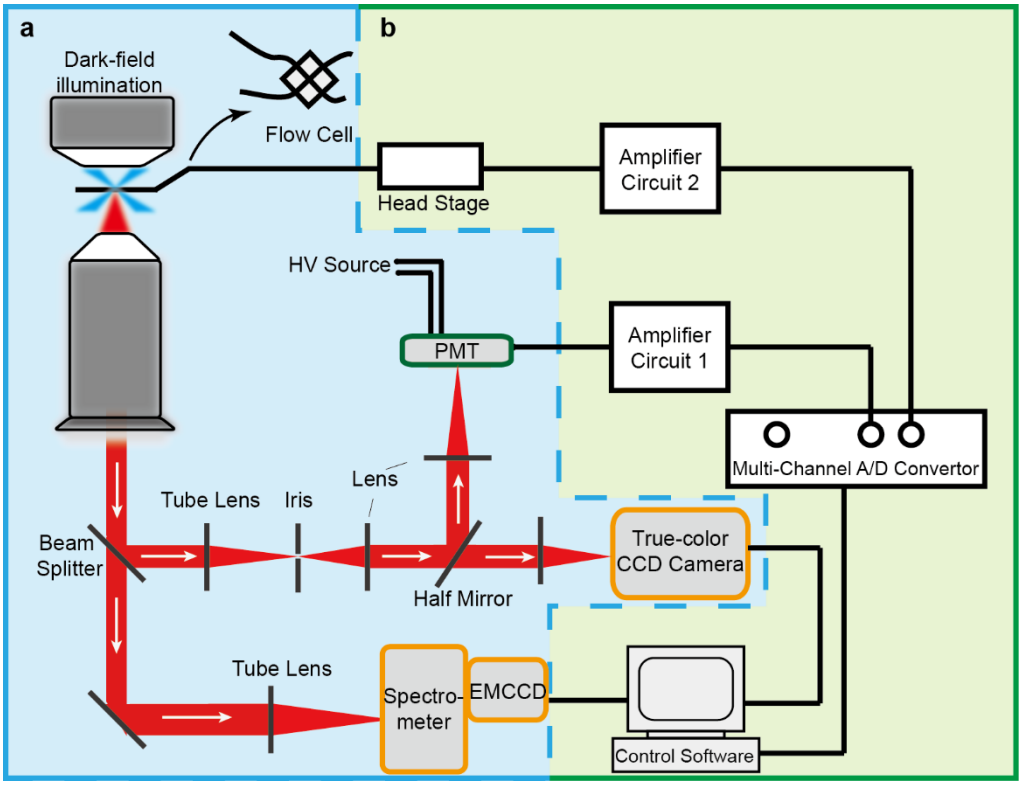

Fig. 1 Schematic of the integrated system. Experimental configuration of the dark-field microscopy system (a) and the homebuilt ultralow ionic current acquisition system (b).

2.1 Optical detection system

A standard dark-field microscopy setup was used for illuminating and monitoring the process

on the nanopore chip. The dark-field illumination is constructed on an inverted microscope (Ti-U, Nikon, Japan). The unpolarized white light from a 100 W halogen lamp is focused on the nanopore chip. The scattered light signal is collected by a 40x objective (NA = 0.8-0.95) from the bottom of the flow cell. The light scattering spectra is dispersed by a Czerny-Turner spectrograph (Isoplane SCT320, Princeton Instrument, US) and recorded by an electron multiplying charge coupled devices array (EMCCD, ProEM, Princeton Instruments, US) camera. High-speed intensity monitoring is achieved by the integration of a lab-designed optical path equipped with a photomultiplier tube (PMT, R921, Hamamatsu, Japan), a lab-made current amplifier and a multichannel data acquisition system. The output image from the microscope is reconstructed on the photosensitive surface of the PMT and the assisted true-color digital CCD camera using lenses. The single-nanopore region is defined by an adjustable iris positioned on the output image plane in the optical path. All of these components are mounted along a common optical axis. The time resolution of the optical signal is determined by the bandwidth of the amplifier and the sampling rate of an analog-digital converter, which was 50 kHz in our experiments. The synchronized collection of electrical and optical signals was guaranteed by the multichannel design of the data acquisition system. Our optical system composes an alternative structure that positions the spectrometer and EMCCD on a branch of the optical path towards the PMT. This configuration ensures the capture of spectra in the regions of interest along with the intensity monitoring. It should be noted that the spectra are recorded at a low sampling rate due to the limitation of speed of the readout from the EMCCD.

For real-time monitoring of the optical intensity in the nanopore region during the experiment, the dark-field condenser and objective lens was adjusted and focused on the nanopore chip. The scattered light was collected by the objective and imaged on the CCD camera. By adjusting the size of the iris and moving the sample stage, the light from a single metal-coated solid-state nanopore could be selected and then detected by a photomultiplier. The assisted true-color digital CCD camera could be used to display the selected region. Through this optical path, 40% of the scattered light could reach the PMT sensing area. After moving and selecting the nanopore area, the optical path could be changed by replacing the 20:80 beam splitter with a mirror and removing the 50:50 beam splitter in the optical path so that all of the scattered light could be detected by the photomultiplier.

2.2 Ultralow current acquisition system

A lab-designed integrated and ultralow current measurement system was employed in the electrical detection. The entire measurement system contains three parts: the headstage, the current amplifier, the filter circuit and the analog-digital converter (ADC). For the headstage, a preamplifier was used to apply a constant potential on both sides of the nanopore and to amplify the ionic current at pico-ampere level with a 100-MΩ high-value feedback transimpedance amplifier circuit. A current amplifier could accomplish the subsequent signal conditioning with multistage amplifier circuits. A 3-pole Bessel low-pass filter was integrated in the current amplifier to eliminate noise. The ADC converted the analog signal into a digital signal so that the computer could acquire and manage the signals.

Our lab-built amplifier exhibited an appropriate current measuring range along with a good temporal resolution and current resolution in the unfiltered mode. The constant potential ranged from -1000 mV to 1000 mV, which was the typical range used in the nanopore experiment. The sampling rate of ADC reached from 10 kHz to 500 kHz to satisfy the requirements of the different analytes. The low-pass Bessel filter, with a range of 1-10 kHz, is preferred for noise reduction of

nanopore detection because of its outstanding feature of whole-band frequency hysteresis. In addition, the shielding cage and grounding solutions were applied in this ultralow current measurement to reduce the various noises.

The lab-made ultralow current measurement system exhibited a performance comparable to that of commercial patch-clamp amplifiers, such as Axopatch 200B and HEKA EPC 10 patch clamp systems, which are commonly used in nanopore analyses. More importantly, the integrated ultralow current measurement system not only gave a signal amplification of the ionic current but also simultaneously achieved the acquisition of PMT signals.

2.3 Metal-coated nanopore and flow cell

Metal-coated solid-state nanopores are fabricated using standard semiconductor processing of silicon chips. Low-stress silicon nitride membranes were covered by an adhesion layer of titanium and gold to generate surface plasmons around the nanopore with a thickness of 10 nm and 90 nm, respectively (Fig. 2b). The metal layer was deposited by electron beam evaporation after being cleaned with oxygen plasma to remove organic contamination. A focus ion beam was used to drill the nanopores with various diameters ranging from 150 nm to 300 nm. A scanning electron micrograph of a typical metal-coated solid-state nanopore is shown in Fig. 2c.

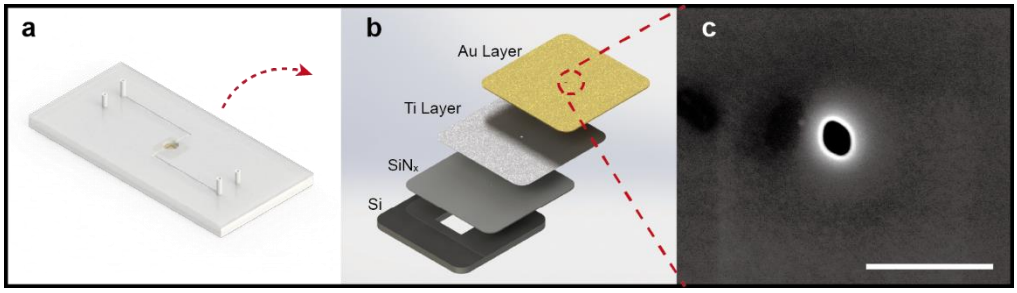

Fig. 2 a) Schematic of the PDMS flow cell for a synchronized optical and electrical readout of a single nanopore. b) Schematic of a metal-coated solid-state nanopore (not to scale). c) Scanning electron micrograph of a typical metal-coated nanopore chip. (scale bar is 500 nm).

To achieve the acquisition of optical and ionic current signals, we designed and fabricated a flow cell containing an optical path for light illumination and acquisition, as well as a pair of chambers to hold the electrolyte solution. A diagram of the flow cell is shown as Fig. 2a. As a first step, two polydimethylsiloxane (PDMS, Sylgard 184, Dow Corning) layers were assembled to form the inlet and outlet channels. The thickness of each layer was less than 1 mm. There are two main reasons to maintain a low thickness of the PDMS layer. First, the edges of the upper chamber are a major source of stray light that significantly reduces the signal-to-noise ratio of the transmitted optical signal in a dark-field illumination. Second, the thickness of the flow cell is limited by the work distance from the dark-field condenser and the objective lenses. The condenser and objective lens with a higher numerical aperture have a shorter work distance. High numerical aperture objective lenses provide a high-resolution in a dark-field imaging system while simultaneously offering fine focusing results for a objective-focused light beam. Thus, it is necessary to design an ultra-thin flow cell. In this study, the entire thickness of the designed flow cell is less than 4 mm. A metal-coated solid-state nanopore chip is sandwiched between the two layers of PDMS. The lower part of PDMS was irreversibly bonded on a standard coverslip (ThermoFisher, US), which was

thoroughly cleaned by ultrasound bath in acetone and deionized water before assembly. The final assembly is achieved by direct positioning the PDMS layer on top of each other and then on the coverslip after exposure in the air plasma. Two Teflon tubes are used for injecting solution into the chamber and holding the electrode.

3 Scattered light and ionic current from the single nanopore

To estimate the applicability of different sizes of nanopores, we fabricated an Au-coated solid-state nanopore array with a diameter ranging from 150 nm to 300 nm. A 100 W halogen light was used for dark-field microscopy and exciting the surface plasmon. Scattered light from each single Au-coated nanopore could be collected by the inverted microscope and detected by the EMCCD. In this approach, the dark-field image and scattered light spectrum could be obtained.

In Fig. 3, we show the representative dark-field images and scattering spectra from single metal-coated nanopores. The nanopores were drilled on an Au layer coated silicon nitride substrate, with diameters ranging from 150 nm to 300 nm (Fig. 3b). A bright reddish spot was observed for each nanopore, and the intensity of diffracted light from the nanopore increased with the diameter, as shown in Fig. 3c. The scattered-light intensity from nanopores with a diameter of 300 nm could reach to approximately ten times higher than that of nanopores with a diameter of 150 nm. The scattering spectrum of each nanopore exhibited a pronounced resonance peak with a maximum intensity at wavelengths varying from 650 nm to 750 nm, depending on the pore diameter. Such a resonance peak could be attributed to the generation of surface plasmons at the edge of the pore[51].

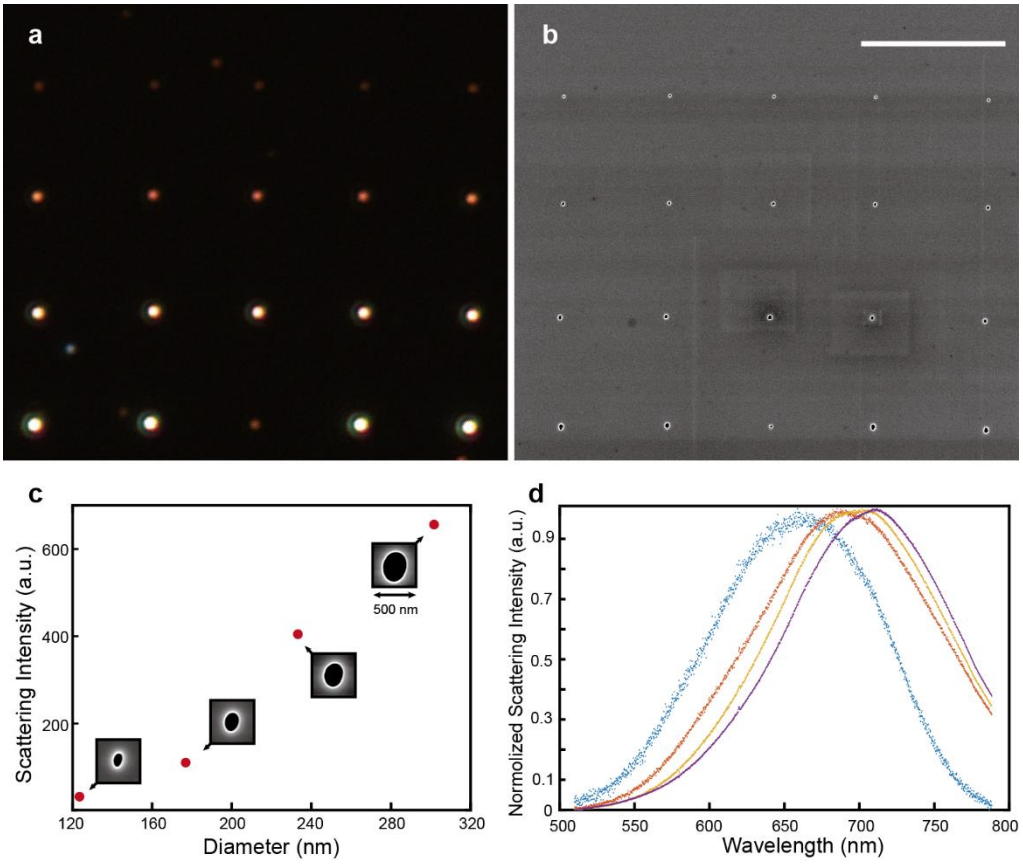

Fig. 3 Characterization of single metal-coated nanopore under a dark field. a) True-color image of single metal-coated nanopores with a diameter of ~150 nm, ~200 nm, ~250 nm and ~300 nm in ambient air. b)

Corresponding scanning electron micrograph for each nanopore array (scale bar is 10 μm). c) Plots of the scattering intensities for each nanopore vs. diameter, which shows the intensities increasing along with an increase in the pore diameters. d) Corresponding scattering spectra for each single metal-coated nanopore with a diameter of 150 nm (blue), 200 nm (red), 250 nm (yellow) and 300 nm (purple), an average of 4 nanopores.

According to the pioneering work, the resonance scattering spectra of nanopores in Au thin-films are qualitatively similar to those measured for Au nanodisks[52]. Using this knowledge, the plasmonic resonance position can be predicted for a single nanopore by calculating the scattering properties of a single nanodisk with the same diameter and height (depth). Fig. 4 shows a series of predicted surface plasmonic resonance spectra of isolated nanodisks, with a height of 90 nm and diameter of 150 nm, 200 nm, and 250 nm, using the discrete dipole approximation (DDA) simulation method. The simulated resonance peaks range from approximately 600 nm to 800nm and red-shift with an increasing diameter of the nanodisk. The difference between the simulated spectra of nanodisks and the experimental results of Au-coated nanopore might be caused by the following factors. First, the geometry of nanopores fabricated by focused ion beam did not be the exactly match the shape we used for the simulation; second, the focused ion beam might induce the redistribution of Au atoms around the nanopore so that a thin layer of Au might form inside the pore and cover the wall of silicon nitride. Hence, a volcano-like structure might be generated inside the pore that could change the dark-field scattering spectrum of the nanopore. Presently, we are working on exploring more suitable methods for predicting the scattering spectra of such metal-coated nanopores.

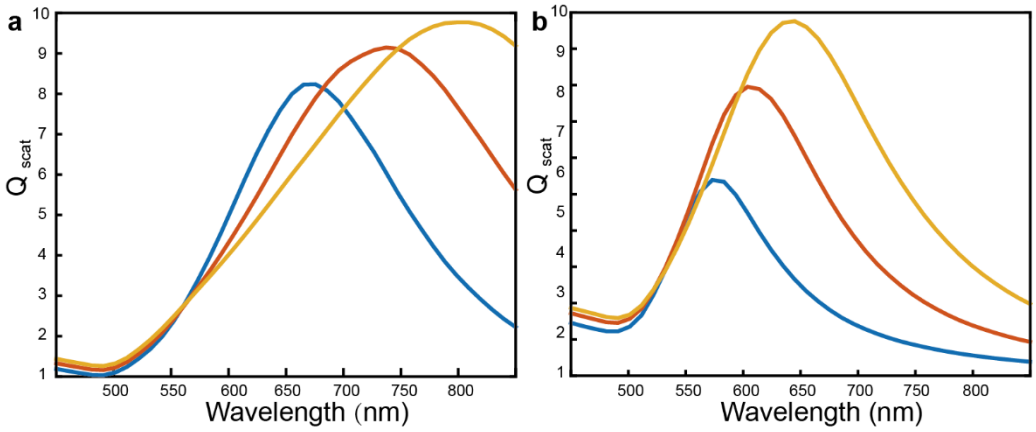

Fig. 4 Simulated scattering spectra of single gold nanodisk with a height of 90 nm and diameter of 150 nm (blue), 200 nm (red) and 250 nm (yellow) in ambient water (a) and air (b). Inset: the size of the DDA target constructed to simulate the scattering spectra of an isolated nanodisk, which could be used to deduce the dark-field spectra of isolated nanopores on Au film.

As previously demonstrated, the diffracted light from a single metal-coated nanopore covers a broad scattering spectrum because of dipole-localized surface plasmons at the edge of the nanopore. When a single analyte moves through the nanopore, the diffracted light behavior changes. To increase the sensitivity of an optical detection system and enlarge the signal variation caused by the translocation events, a reflected dark-field illumination method with a laser beam as the excitation light source could be used (Fig. 5). Briefly, we replace the halogen light source and the dark-field

condenser with the beam of a He-Ne laser. While the background light is reflected by the Au layer, a part of the monochromatic light can be diffracted through the metal-coated nanopore. Thus, a bright reddish spot could be observed on a CCD camera or detected by a photomultiplier. The dark-field image under laser illumination is shown in Fig. 5b. The intensity of each spot clearly depends on the size of each circular aperture.

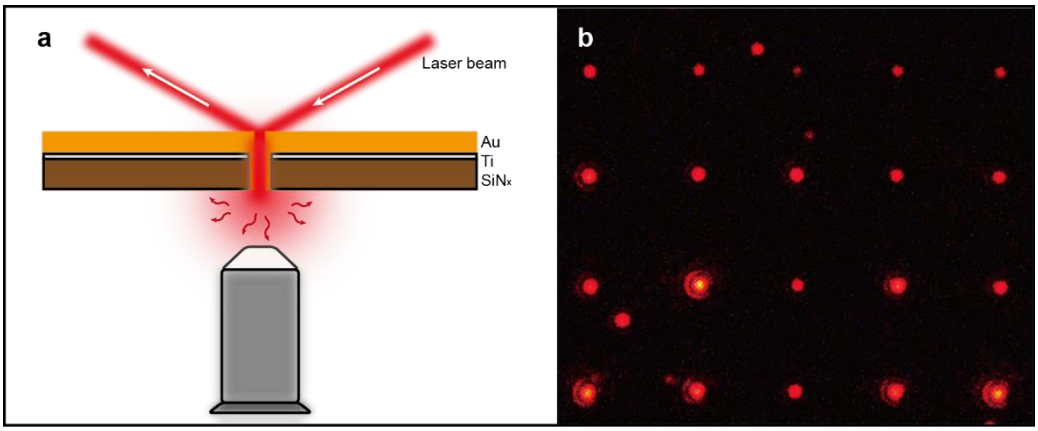

Fig. 5 a) Schematic of reflected dark-field illumination method for detecting a single nanopore. b) True–color image of the same nanopore array corresponding to Fig. 3, under reflected dark-field illumination.

To investigate the feasibility of this method for synchronized optical and electrical detection of the translocation events, we measured the baseline ionic current recorded by the current head stage with a pair of Pt electrodes and recorded the light scattering from a single nanopore with a photomultiplier. The ionic current and scattered light from a single nanopore was monitored simultaneously. The ionic current signal was low-pass filtered at 10 kHz before digitization at 50 kHz (Fig. 6a). Synchronized optical and electrical data acquisition was achieved using a multichannel-designed analog-digital converter (Axon Digidata 1550, Molecular Devices). The internal clock of the analog-digital converter ensures simultaneous data acquisition. Alternatively, we also examined the possibility of using a data acquisition board (PCI 6351, Nation Instruments) with a custom LabVIEW program to achieve the synchronized optical and electrical measurements.

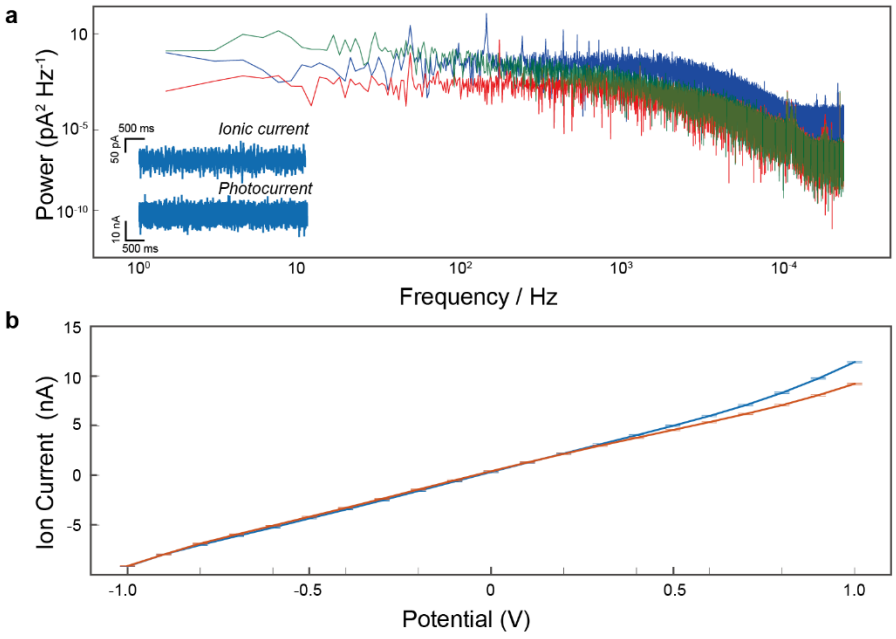

Fig. 6 a) Power spectral densities of ionic current detected from a single Au-coated nanopore, before (red) and after (green) turning on the halogen light, and from a single nanopore without Au layer in a conventional flow cell (blue). Inset: baseline ionic current at 0 mV, under white light illumination for a single 150 nm Au-coated nanopore, and baseline photocurrent from PMT at 1100 mV of the same nanopore at the same period time. b) Ionic current-voltage characteristics of a single Au-coated nanopore with (blue) and without (red) white light illumination. The error bars presents standard deviations of 1-s sampling traces under different bias. The light-induced effects of ionic current through the nanopore might mainly originate from the plasmonic enhanced heat effects and plasmoelectric potential.

The dark-field imaging reported in this study was achieved using a dark-field condenser and 100 W halogen lamp. The scattered light transmitted through an Au-coated nanopore was collected by the objective lens, then the photocurrent was generated by the photomultiplier. The photocurrent was monitored by the data acquisition system with a sampling rate of 50 kHz and was then sent to the computer and simultaneously recorded with the ionic signal. In our experiment, the photocurrent generated by the scattered light from a single 150 nm Au-coated nanopore was typically 50 nA when illuminated by the halogen lamp (Fig. 6a).

The noise power spectrum density (PSD) of the nanopore measurements could help analyze noise conditions for the nanopore. Previous research showed that there is flicker noise (1/f noise) that exists in the low frequency region (freq. <1 kHz) because of the electrolyte solution fluctuations in the detection cell. Generally， for SiN_x solid-state nanopores, the flicker noise power density is less than 1 pA^2/Hz at 1 Hz (the blue and red folding line of Fig. 6a). During the synchronized optical and electrical measurements, the flicker noise level increased after turning on the illuminating white lamp. The reason might be the heat effect under light illumination, especially at the nanopore region because of the generation of surface plasmons.

Compared with the bare SiN_x solid-state nanopore, the Au coating might be able to suppress the white noise with frequency between 10 kHz and 100 kHz. Compared with the power spectral density of bare SiN_x nanopore, which exhibits a white noise region with a similar power to the 1/f noise, the white noise of an Au-coated nanopore decreases in a long range of frequency. However, as previously discussed, the illumination of white light increases the low-frequency noise of the ionic current. The decrease of higher frequency enables the achievement of a standard solid-state nanopore experiment with our integrated system.

Fig. 6b shows current-voltage characteristics of ionic current with and without illumination by a halogen lamp. According to the previous work, the diameter a solid-state nanopore could be estimated by the current-voltage curve using the following equation[53]:

$$G = \sigma \frac{\pi d^2}{4l}$$

where G is the open pore conductance values, σ is the conductivity of bulk solution (0.13 s/m for 10 mM KNO_3 solution, measured by DDSJ-318 conductivity meter, INESA Instrument), l is the length of the nanopore, i.e., the thickness of the membrane, and d is the diameter of the circular pore. The estimated diameter of the Au-coated nanopore in Fig. 6b is 130 nm, which is smaller than the SEM results. This is reasonable because the equation is more applicable to smaller solid-state nanopores. In addition, although there are more precise and complicated equations to model the relativity between conductance and nanopore diameter, the role of such an Au layer is remains unclear. The current-voltage curve exhibits good linearity for the experimental voltage (-1.0 V to

1.0 V). During illumination by the halogen lamp, a small change of ionic current could be observed especially under the positive bias (0.5-1.0 V). This might be the result of the surface plasmon induced heat effect[57-59] and plasmoelectric potential induced by the incident light[60]. The results show that the noise introduced by illumination by white light has limited influence on the ionic current detection. Therefore, our integrated system that includes the metal-coated nanopore and the optical and electrical acquisition system, exhibits acceptable performance for both optical and electrical detection.

4 Conclusion

The present work demonstrates a novel integrated system for synchronized optical and electronic detection of nanopore translocation events. A metal-coated nanopore was fabricated on a silicon nitride substrate and assembled into a transparent flow cell. A dark-field microscopy system equipped with a high-speed optical intensity monitoring detector and an ultra-low current high-speed data acquisition system was designed for monitoring the scattering light and ionic current signal from the nanopore. Because of the plasmonic effect at the edge of the metal nanopore induced by the incident light, the single solid-state nanopore could be observed easily under the dark-field microscope, without introducing additional fluorescent dye or a labeling procedure. With this system, the ionic current and elastic scattering signal could be detected simultaneously with a sampling rate of 10 to 100 kHz. We were able to regulate the scattering spectra of a single metal-coated nanopore with the diameter of the nanopore, and the elastic scattering spectrum of a single pore could be predicted by the discrete dipole approximation simulation method. This system could provide a potential approach to simultaneously acquire electrical information, such as the charge, and optical information, including the refractive index, along with the single-analyte translocation process through the nanopore. At this stage, the system only achieves to monitor the ionic current through a single nanopore together with the recording of the light scattering. In future, the integration of the multiplexing ionic current readouts with the optical detection will be of benefit to realize the parallel measurements of the current and light in multiple nanopores.

Using the interaction of surface plasmons between the single nanoparticle and the metal-coated nanopore, we are working on obtaining the single metal nanoparticle translocation events through the plasmonic nanopore by monitoring the variation of scattered light from the plasmonic nanopore. Furthermore, this novel integrated system based on the metal-coated nanopore also introduces new approaches for optical detection, including label-free detection of single-molecule events and the interaction process between biomolecules. Based on our plasmonic nanopore system, multiple types of plasmon-based optical detection methods including not only the Rayleigh scattering from a single nanopore but also surface-enhanced Raman spectroscopy[35] and plasmon-enhanced fluorescence[54-56] can be performed.

Acknowledgment

This research was supported by the National Basic Research Program of China (2011CB707605), the National Natural Science Foundation of China (21327807, 21421004, 21125522), Shanghai Pujiang Program (12JC1403500), and Program for Professor of Special Appointment (Eastern Scholar) at Shanghai Institutions of Higher Learning (YJ0130504).

Reference

1. J. Shendure and H. Ji, *Nat Biotech*, 2008, **26**, 1135-1145.
2. D. Branton, D. W. Deamer, A. Marziali, H. Bayley, S. A. Benner, T. Butler, M. Di Ventra, S. Garaj, A. Hibbs and X. Huang, *Nature biotechnology*, 2008, **26**, 1146-1153.
3. G. F. Schneider and C. Dekker, *Nature biotechnology*, 2012, **30**, 326-328.
4. Y.-L. Ying, D.-W. Li, Y. Liu, S. K. Dey, H.-B. Kraatz and Y.-T. Long, *Chemical Communications*, 2012, **48**, 8784-8786.
5. C. Cao, Y.-L. Ying, Z. Gu and Y.-T. Long, *Analytical chemistry*, 2014.
6. H.-Y. Wang, Z. Gu, C. Cao, J. Wang and Y.-T. Long, *Analytical chemistry*, 2013, **85**, 8254-8261.
7. Y.-L. Ying, C. Cao and Y.-T. Long, *Analyst*, 2014, **139**, 3826-3835.
8. Y. Liu, Y.-L. Ying, H.-Y. Wang, C. Cao, D.-W. Li, W.-Q. Zhang and Y.-T. Long, *Chemical Communications*, 2013, **49**, 6584-6586.
9. Y.-L. Ying, J. Zhang, F.-N. Meng, C. Cao, X. Yao, I. Willner, H. Tian and Y.-T. Long, *Scientific reports*, 2013, **3**.
10. Y. L. Ying, J. Zhang, R. Gao and Y. T. Long, *Angewandte Chemie International Edition*, 2013, **52**, 13154-13161.
11. S. Howorka and Z. Siwy, *Chemical Society Reviews*, 2009, **38**, 2360-2384.
12. B. N. Miles, A. P. Ivanov, K. A. Wilson, F. Doğan, D. Japrung and J. B. Edel, *Chemical Society reviews*, 2013, **42**, 15-28.
13. M. Firnkes, D. Pedone, J. Knezevic, M. Döblinger and U. Rant, *Nano letters*, 2010, **10**, 2162-2167.
14. J. J. Kasianowicz, E. Brandin, D. Branton and D. W. Deamer, *Proceedings of the National Academy of Sciences*, 1996, **93**, 13770-13773.
15. M. Pastoriza-Gallego, L. Rabah, G. Gibrat, B. Thiebot, F. o. G. van der Goot, L. Auvray, J.-M. Betton and J. Pelta, *Journal of the American Chemical Society*, 2011, **133**, 2923-2931.
16. E. A. Manrao, I. M. Derrington, A. H. Laszlo, K. W. Langford, M. K. Hopper, N. Gillgren, M. Pavlenok, M. Niederweis and J. H. Gundlach, *Nature biotechnology*, 2012, **30**, 349-353.
17. T. Z. Butler, M. Pavlenok, I. M. Derrington, M. Niederweis and J. H. Gundlach, *Proceedings of the National Academy of Sciences*, 2008, **105**, 20647-20652.
18. M. M. Mohammad, R. Iyer, K. R. Howard, M. P. McPike, P. N. Borer and L. Movileanu, *Journal of the American Chemical Society*, 2012, **134**, 9521-9531.
19. D. Wendell, P. Jing, J. Geng, V. Subramaniam, T. J. Lee, C. Montemagno and P. Guo, *Nature nanotechnology*, 2009, **4**, 765-772.
20. H.-Y. Wang, Y. Li, L.-X. Qin, A. Heyman, O. Shoseyov, I. Willner, Y.-T. Long and H. Tian, *Chem. Commun.*, 2013, **49**, 1741-1743.
21. C. Dekker, *Nature nanotechnology*, 2007, **2**, 209-215.
22. A. J. Storm, J. H. Chen, X. S. Ling, H. W. Zandbergen and C. Dekker, *Nat Mater*, 2003, **2**, 537-540.
23. B. M. Venkatesan, A. B. Shah, J. M. Zuo and R. Bashir, *Advanced functional materials*, 2010, **20**, 1266-1275.
24. S. Garaj, W. Hubbard, A. Reina, J. Kong, D. Branton and J. Golovchenko, *Nature*, 2010, **467**, 190-193.

25. G. F. Schneider, S. W. Kowalczyk, V. E. Calado, G. Pandraud, H. W. Zandbergen, L. M. Vandersypen and C. Dekker, *Nano letters*, 2010, **10**, 3163-3167.
26. C. A. Merchant, K. Healy, M. Wanunu, V. Ray, N. Peterman, J. Bartel, M. D. Fischbein, K. Venta, Z. Luo and A. C. Johnson, *Nano letters*, 2010, **10**, 2915-2921.
27. T. Osaki, H. Suzuki, B. Le Pioufle and S. Takeuchi, *Anal Chem*, 2009, **81**, 9866-9870.
28. G. Baaken, N. Ankri, A.-K. Schuler, J. r. Rühe and J. C. Behrends, *Acs Nano*, 2011, **5**, 8080-8088.
29. N. A. W. Bell, V. V. Thacker, S. Hernandez-Ainsa, M. E. Fuentes-Perez, F. Moreno-Herrero, T. Liedl and U. F. Keyser, *Lab on a chip*, 2013, **13**, 1859-1862.
30. A. Kleefen, D. Pedone, C. Grunwald, R. Wei, M. Firnkes, G. Abstreiter, U. Rant and R. Tampé, *Nano letters*, 2010, **10**, 5080-5087.
31. B. McNally, A. Singer, Z. Yu, Y. Sun, Z. Weng and A. Meller, *Nano Lett*, 2010, **10**, 2237-2244.
32. J. Larkin, M. Foquet, S. W. Turner, J. Korlach and M. Wanunu, *Nano letters*, 2014, **14**, 6023-6029.
33. M. Urban, A. Kleefen, N. Mukherjee, P. Seelheim, B. Windschiegl, M. Vor der Brüggen, A. Koçer and R. Tampé, *Nano letters*, 2014, **14**, 1674-1680.
34. G. A. Chansin, R. Mulero, J. Hong, M. J. Kim, A. J. Demello and J. B. Edel, *Nano Lett*, 2007, **7**, 2901-2906.
35. M. P. Cecchini, A. Wiener, V. A. Turek, H. Chon, S. Lee, A. P. Ivanov, D. W. McComb, J. Choo, T. Albrecht and S. A. Maier, *Nano Lett*, 2013, **13**, 4602-4609.
36. A. Demuro and I. Parker, *Cell Calcium*, 2003, **34**, 499-509.
37. A. Ivankin, R. Y. Henley, J. Larkin, S. Carson, M. L. Toscano and M. Wanunu, *ACS nano*, 2014, **8**, 10774-10781.
38. B. N. Anderson, O. N. Assad, T. Gilboa, A. H. Squires, D. Bar and A. Meller, *ACS nano*, 2014, **8**, 11836-11845.
39. S. Liu, Y. Zhao, J. W. Parks, D. W. Deamer, A. R. Hawkins and H. Schmidt, *Nano Lett*, 2014, **14**, 4816-4820.
40. W. H. Pitchford, H.-J. Kim, A. P. Ivanov, H.-M. Kim, J.-S. Yu, R. J. Leatherbarrow, T. Albrecht, K.-B. Kim and J. B. Edel, *ACS nano*, 2015, **9**, 1740-1748.
41. C. Genet and T. Ebbesen, *Nature*, 2007, **445**, 39-46.
42. H. Bethe, *Physical Review*, 1944, **66**, 163-182.
43. E. Betzig and J. K. Trautman, *Science*, 1992, **257**, 189-195.
44. T. W. Ebbesen, H. Lezec, H. Ghaemi, T. Thio and P. Wolff, *Nature*, 1998, **391**, 667-669.
45. H. J. Lezec, A. Degiron, E. Devaux, R. Linke, L. Martin-Moreno, F. Garcia-Vidal and T. Ebbesen, *Science*, 2002, **297**, 820-822.
46. M. J. Levene, J. Korlach, S. W. Turner, M. Foquet, H. G. Craighead and W. W. Webb, *Science*, 2003, **299**, 682-686.
47. J. Eid, A. Fehr, J. Gray, K. Luong, J. Lyle, G. Otto, P. Peluso, D. Rank, P. Baybayan and B. Bettman, *Science*, 2009, **323**, 133-138.
48. A. G. Brolo, R. Gordon, B. Leathem and K. L. Kavanagh, *Langmuir*, 2004, **20**, 4813-4815.
49. T. Rindzevicius, Y. Alaverdyan, A. Dahlin, F. Höök, D. S. Sutherland and M. Käll, *Nano letters*, 2005, **5**, 2335-2339.
50. F. Nicoli, D. Verschueren, M. Klein, C. Dekker and M. P. Jonsson, *Nano letters*, 2014, **14**, 6917-6925.

51. E. Popov, N. Bonod, M. Nevière, H. Rigneault, P.-F. Lenne and P. Chaumet, *Applied optics*, 2005, **44**, 2332-2337.
52. J. Prikulis, P. Hanarp, L. Olofsson, D. Sutherland and M. Käll, *Nano Letters*, 2004, **4**, 1003-1007.
53. S. W. Kowalczyk, A. Y. Grosberg, Y. Rabin and C. Dekker, *Nanotechnology*, 2011, **22**, 315101.
54. A. G. Brolo, S. C. Kwok, M. G. Moffitt, R. Gordon, J. Riordon and K. L. Kavanagh, *Journal of the American Chemical Society*, 2005, **127**, 14936-14941.
55. H. Aouani, O. Mahboub, E. Devaux, H. Rigneault, T. W. Ebbesen and J. Wenger, *Nano letters*, 2011, **11**, 2400-2406.
56. H. Aouani, O. Mahboub, N. Bonod, E. Devaux, E. Popov, H. Rigneault, T. W. Ebbesen and J. Wenger, *Nano letters*, 2011, **11**, 637-644.
57. U. F. Keyser, D. Krapf, B. N. Koeleman, R. M. Smeets, N. H. Dekker and C. Dekker, Nano letters, 2005, **5**, 2253-2256.
58. M. P. Jonsson and C. Dekker, Nano letters, 2013, **13**, 1029-1033.
59. C. R. Crick, P. Albella, B. Ng, T. Roschuk, A. P. Ivanov, M. Cecchini, F. Bresme, S. A. Maier and J. B. Edel, Nano letters, 2015. DOI: 10.1021/nl504536j
60. M. T. Sheldon, J. Van de Groep, A. M. Brown, A. Polman and H. A. Atwater, science, 2014, **346**, 828-831.